American Mineralogist, Volume 76, pages 1141–1152, 1991

Crystal chemistry of clinopyroxenes from mantle eclogites: A study of the key role of the M2 site population by means of crystal-structure refinement

ROBERTA OBERTI
C.N.R., C.S. Cristallografia Strutturale, via Bassi 4, I-27100 Pavia, Italy
FLORIE A. CAPORUSCIO*
Dipartimento di Scienze della Terra, Università di Pavia, via Bassi 4, I-27100 Pavia, Italy

ABSTRACT

Single-crystal X-ray structure refinements of a series of geochemically well-characterized clinopyroxenes from grospydite and eclogite xenoliths from the Roberts Victor and Bobbejaan diamond mines, South Africa, have been carried out. The study was done to clarify the crystal chemical relations of high-pressure mantle clinopyroxenes and to understand the structural constraints on REE substitution. The jadeite component ranges from 0 to 50 mol%, and cation vacancies are suggested from EMP analyses.

All the omphacitic clinopyroxenes examined belong to the *C*2/*c* space group, in agreement with the high temperature of reequilibration and the rapid quenching during kimberlite transport. Relatively high (Fe^{2+} + Mg) contents (up to 0.19 apfu) are present at the M2 site in many of these specimens, resulting in a volume contraction in the M2 polyhedron. The presence of vacancies doesn't significantly affect the M2 site volume. The overall decrease in the unit-cell volume observed in vacancy-bearing pyroxenes is predominantly caused by the contraction in the M1 polyhedron, resulting from the incorporation of highly charged cations in M1 required to preserve overall charge balance of the structure. Both the chemical substitutions observed at M2 [Ca → (Fe^{2+}, Mg) and Na → vacancy] are therefore efficient ways to allow crystallization of low-volume clinopyroxene. Other crystal chemical features are similar to those reported for metamorphic eclogite clinopyroxenes on the Di-Jd join.

Variations in cation electrostatic potentials, volume, and shape of the M2 polyhedron caused by major elements agree with the observed inverse relationship between Na content and total trivalent REE concentration.

INTRODUCTION

The crystal chemical relations of high-pressure clinopyroxenes have significance for other aspects of pyroxene geochemistry (Prewitt, 1980; Rossi, 1988). Until recently, there has been a paucity of crystal structure refinement data for naturally occurring, high-pressure mantle clinopyroxenes. Three studies have accounted for a total of 14 clinopyroxene samples. Smith et al. (1982) described the crystal-chemical features of two vacancy-bearing pyroxenes from grospydites in the Zagadochnaya kimberlite of Russia. Dal Negro et al. (1984) refined the structures of 11 diopsidic Ca- and Ts-bearing clinopyroxenes from spinel lherzolite nodules found in the Newer Volcanics basanites of Victoria, Australia. In an article concerning nonstoichiometric clinopyroxenes, McCormick (1986) refined the crystal structure of a cation vacancy-bearing pyroxene from a kyanite eclogite xenolith from Bellsbank kimberlite, South Africa.

The present study concerns ten clinopyroxenes along the diopside-jadeite (Di-Jd) join from mantle eclogite xenoliths (nine bimineralic and one grospyditic) from the Bobbejaan and Roberts Victor diamond mines, South Africa. The samples are of special interest, since they have been characterized using a variety of geochemical techniques (Caporuscio, 1988). Data were obtained for major and rare earth element (REE) contents, oxygen isotopes, and radiogenic isotopes (Rb/Sr, Nd/Sm).

The primary objective of this study is to characterize the crystal chemical features of a group of petrogenetically related, high-pressure mantle clinopyroxenes. Samples were chosen with Na contents in the range 0.05–0.50 atoms per formula unit (apfu), thus covering a compositional range previously unstudied. Some specimens with vacancies at the M2 site have been chosen in order to obtain a fuller understanding of the related structural modifications.

The second topic is pyroxene crystal-chemical controls on REE substitution. Examination of the ionic radii values published by Shannon (1976) suggests that the REE can most readily substitute into the M2 site of clinopy-

---

* Present address: United States Environmental Protection Agency, Region II, AWM-RAD, 26 Federal Plaza, New York, New York 10278, U.S.A.

0003–004X/91/0708–1141$02.00

roxenes. The ionic radii of lanthanides range in eightfold coordination from 0.98 Å (Yb) to 1.16 Å (La), and therefore they can, in principle, be incorporated in the M2 site, which is predominantly occupied by Ca (1.12 Å) and Na (1.18 Å). It is most unlikely that the REE, whose ionic radii in octahedral coordination vary from 0.87 Å (Yb) to 1.03 Å (La), could enter the M1 site, in which the ionic radii of the major elements range from 0.53 (Al^{3+}) to 0.78 Å (Fe^{2+}). On the other hand, Caporuscio and Smyth (1986, 1990) have suggested that the total amount of REE accepted into the M2 site is controlled by the electrostatic site potential, which is inversely related to the amount of Na in the M2 site.

Particular attention has, therefore, been paid to the changes in the M2 site geometry resulting from changes in major element composition, in order to detect geometrical or site potential constraints that might affect REE substitution.

SAMPLE DESCRIPTION

Overview

The Bobbejaan (SBB) and Roberts Victor (SRV and XM) mines in South Africa are noted for their predominantly eclogitic nodule suites, which have been the subject of numerous petrologic studies (Dawson, 1980; Dawson and Gurney, 1987; Caporuscio, 1988). A suite of over 70 eclogite samples from these mines has been analyzed by electron microprobe (EMP) at Los Alamos National Laboratory (Smyth and Caporuscio, 1984). From this sample suite, ten eclogitic pyroxenes, which represent the full range of bimineralic and grospyditic compositions, were selected for single-crystal X-ray refinement. A petrographic description is given in Appendix 1.

Previous researchers (Smyth and Caporuscio, 1984; McCormick and Smyth, 1986) have estimated that the samples crystallized at pressures of 30–50 kbar and temperatures of 1350–1550 °C, followed by subsolidus reequilibration and recrystallization at pressures of 30–40 kbar and temperatures of 950–1200 °C, processes that have modified textures and primary phase compositions.

Major element compositions and crystallization sequence

Major element compositions of the pyroxenes are given in Table 1; microprobe operating procedures are detailed in Smyth and Caporuscio (1984). The pyroxenes analyzed are internally homogeneous, with chemical zoning only in distinct rim regions. Major element compositions were recast into end-member percentages using the computer program PYROS (Smyth, 1980) and are listed in Table 1. The end-member pyroxene components show significant variations: in particular, jadeite values range from 0 (SRV-4) to 50 mol% (SBB-2H). The jadeite content of the pyroxenes has been interpreted to indicate the crystallization sequence of eclogites by Smyth et al. (1989). Pyroxene with the highest Al content would be the first phase to crystallize (along with corundum) and upon subsolidus reequilibration would produce a corundum grospydite (sample SBB-2H). At the point in the crystallization sequence where garnet would begin to nucleate, one may still expect minor garnet exsolution from Al-saturated clinopyroxene (sample SBB-61). The next garnets to crystallize would be very Fe rich, and the pyroxenes would have moderate jadeite contents (e.g., sample SBB-25). Continued crystallization would progressively drive the fractionation sequence toward Mg-rich bulk rock compositions with low jadeite content in the pyroxenes (samples SBB-37 and, finally, SRV-4).

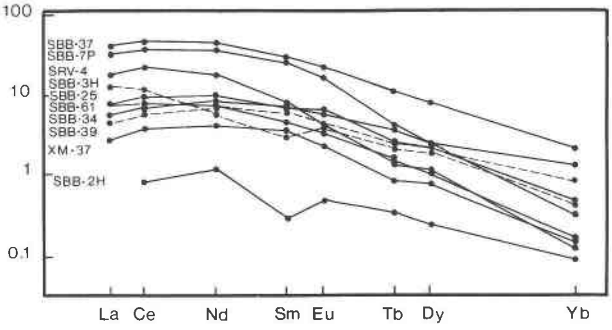

Fig. 1. Clinopyroxene chondrite-normalized REE patterns. Total REE concentrations are correlated with the Na contents of the clinopyroxenes. The analysis of Ce for sample SBB-2H was obtained by ion probe at the C.S. Cristallografia Strutturale, Pavia.

Rare earth element compositions

Instrumental neutron activation analyses (INAA) of the pyroxenes for REE were carried out at the Lunar and Planetary Laboratory, University of Arizona. General operating procedures of this system are described by Boynton (1979), and specific details are given in Caporuscio (1988). Values of the REE in ppm are listed in Table 2, as are La/Yb ratios, which range from 5.5 (sample SBB-34) to 265.3 (sample SBB-7P).

In a chondrite-normalized REE diagram (Fig. 1), the clinopyroxenes show a general trend of light REE (LREE) enrichment and heavy REE (HREE) depletion. Chondrite-normalized values of La are commonly less than Ce and Nd so that the trend from LREE to HREE is not quite linear. In addition, the grospyditic pyroxene sample and bimineralic sample with garnet exsolution (SBB-2H and SBB-3H, respectively) have peculiar middle REE (MREE) enrichments (Nd, Eu) and depletion (Sm). This type of REE trend is similar to that of Ca- and Al-rich pyroxenes experimentally crystallized from a basaltic melt at 30 kbar (Shimizu, 1980). The overall patterns in Figure 1 are strikingly similar to clinopyroxene REE trends observed in other natural high-pressure eclogitic pyroxenes (Shervais et al., 1988; Early, 1971).

Subtle variations in clinopyroxene LREE relative concentrations are most probably due to competition with cocrystallizing garnet. Crystal-liquid (Irving, 1978; Hanson, 1980) and experimental (Shimizu, 1980) clinopyrox-

TABLE 1. Electron microprobe analyses

	SRV 4	SBB 7P	SBB 37	SBB 34	SBB 3H	SBB 39	SBB 25	SBB 61	XM 37	SBB 2H
Wt% oxides										
SiO_2	54.31	53.79	55.41	54.77	55.89	55.61	55.96	56.70	56.10	54.80
Al_2O_3	1.38	2.54	4.55	5.39	6.39	6.18	7.94	12.42	14.10	16.10
TiO_2	0.07	0.00	0.29	0.16	0.15	0.21	0.43	0.30	0.38	0.07
Cr_2O_3	0.00	3.09	0.18	0.00	0.05	0.10	0.19	0.09	0.15	0.03
Fe_2O_3	1.79	1.92	1.15	1.09	0.00	0.00	0.00	0.00	0.00	1.06
FeO	1.55	0.00	1.70	5.43	4.11	8.09	4.87	2.56	2.54	0.00
MgO	16.96	15.39	15.40	13.28	12.06	12.28	12.24	8.85	7.72	7.10
MnO	0.07	0.07	0.01	0.26	0.02	0.45	0.10	0.04	0.02	0.02
CaO	23.29	19.99	18.48	15.84	16.65	13.34	14.23	12.43	11.86	12.20
Na_2O	0.64	2.57	2.95	3.34	3.77	3.86	4.37	5.91	6.99	8.10
K_2O	0.11	0.00	0.00	0.16	0.00	0.11	0.08	0.07	0.29	0.00
Total	100.17	99.36	100.12	99.72	99.09	100.23	99.96	99.37	100.15	99.50
Cations/six O atoms										
Si	1.969	1.958	1.981	1.987	2.017	2.008	1.999	1.997	1.966	1.924
$^{[4]}Al$	0.031	0.042	0.019	0.013	0.000	0.000	0.001	0.003	0.034	0.076
$^{[6]}Al$	0.028	0.067	0.173	0.217	0.288	0.271	0.314	0.513	0.548	0.590
Ti	0.002	0.000	0.008	0.004	0.004	0.006	0.012	0.008	0.010	0.000
Cr	0.000	0.088	0.005	0.000	0.001	0.003	0.005	0.003	0.004	0.000
Fe^{3+}	0.049	0.053	0.031	0.030	0.000	0.000	0.000	0.000	0.000	0.028
Fe^{2+}	0.047	0.000	0.051	0.165	0.124	0.244	0.145	0.075	0.074	0.000
Mg	0.917	0.835	0.821	0.718	0.649	0.661	0.652	0.465	0.403	0.372
Mn	0.002	0.001	0.000	0.008	0.001	0.014	0.003	0.001	0.001	0.000
Ca	0.905	0.780	0.708	0.616	0.644	0.516	0.545	0.469	0.445	0.459
Na	0.045	0.181	0.204	0.235	0.264	0.270	0.303	0.404	0.475	0.551
K	0.005	0.000	0.000	0.007	0.000	0.005	0.004	0.003	0.013	0.000
vac. (□)	0.000	0.000	0.000	0.000	0.025	0.010	0.017	0.059	0.026	0.000

Note: Analyses for SBB samples from Smyth and Caporuscio (1984), for SRV from Caporuscio (1988), and for XM from McCormick and Smyth (personal communication, Fe as FeO).

ene REE K_d values suggest a preference by the solid phase for MREE. Since all the samples of this study are considered to come from a common (or closely related) igneous fractionally crystallized source (Smyth et al., 1989), the results of Figure 1 can be explained in terms of relative K_d values and mineral phase competition. The preference for MREE ($K_d > 1$) exhibited by clinopyroxene is clearly seen when it is the only crystallizing phase (sample SBB-2H). When garnet and pyroxene are first together on the liquidus, the Ca-rich garnet (X site radius = 0.965 Å) accepts HREE and MREE (Caporuscio and Smyth, 1990), making a high relative proportion of LREE available to clinopyroxene (K_d values near 1). As crystallization continues toward Fe-rich compositions and the liquid is enriched in LREE, still higher relative amounts of the LREE (SBB-37, SBB-7P) can enter the clinopyroxene. The final Mg-rich, Na-poor clinopyroxene (sample SRV-4) does not need to have such an extreme LREE relative enrichment, since the magma should be depleted in those elements by then.

The patterns of Figure 1 suggest a steady decrease in total REE concentrations of the clinopyroxene as jadeite content increases. This is confirmed in Figure 2, in which the total Na content at M2 is used as the abscissa, in that it is actually the main factor affecting both charge and mean bond distances. The observed correlation ($R = 0.913$ when excluding samples SBB-7P and SBB-37) suggests that there is a strong major element crystal-chemical control; the deviation of sample SBB-7P from the correlation is probably related to its high Cr_2O_3 content, which may

TABLE 2. REE contents (ppm) for the clinopyroxene samples

	SRV 4	SBB 7P	SBB 37	SBB 34	SBB 3H	SBB 39	SBB 25	SBB 61	XM 37	SBB 2H
La	4.54	7.96	9.62	1.44	3.36	1.13	2.05	2.11	0.68	n.a.
Ce	13.20	26.29	33.92	5.22	6.87	4.08	6.23	5.90	2.39	0.50
Nd	8.94	18.52	24.94	4.83	2.34	3.58	5.07	4.15	2.09	0.58
Sm	1.42	4.17	5.03	1.15	0.46	0.92	1.22	0.80	0.58	0.04
Eu	0.27	0.95	1.44	0.37	0.23	0.27	0.37	0.23	0.15	0.03
Tb	0.06	0.16	0.46	0.14	0.08	0.09	0.09	0.07	0.03	0.03
Dy	0.33	1.60	3.39	0.66	0.47	0.80	0.73	0.60	0.21	0.23
Yb	0.02	0.03	0.36	0.26	0.09	0.15	0.09	0.03	0.02	0.02
Lu	0.00	0.01	0.03	0.03	0.01	0.02	0.01	0.01	0.02	0.00
La/Yb	227.0	265.3	26.7	5.5	37.3	7.5	22.8	70.3	34.0	n.s.
ΣREE^{3+*}	28.19	57.14	74.37	13.07	13.21	9.97	14.77	13.06	5.81	2.04

* Trivalent REE only summed; Eu excluded because of uncertain oxidation state.

Table 3. Unit-cell parameters and selected crystal data

	SRV 4	SBB 7P	SBB 37	SBB 34	SBB 3H	SBB 39	SBB 25	SBB 61	XM 37	SBB 2H
a (Å)	9.739	9.693	9.678	9.662	9.654	9.644	9.628	9.561	9.551	9.545
b (Å)	8.913	8.889	8.853	8.841	8.831	8.820	8.808	8.730	8.724	8.713
c (Å)	5.253	5.253	5.255	5.253	5.255	5.256	5.254	5.249	5.247	5.246
β (°)	106.02	106.34	106.52	106.78	106.52	107.04	106.88	107.00	106.97	106.90
V (Å^3)	438.3	434.3	431.6	429.6	429.5	427.4	426.4	419.0	418.2	417.4
No. I_{obs}	599	574	583	540	580	537	533	551	558	564
No. I_{all}	649	642	640	637	635	631	623	612	611	612
R_{obs}	0.011	0.013	0.016	0.012	0.013	0.013	0.011	0.010	0.011	0.016
R_{all}	0.012	0.016	0.019	0.016	0.016	0.018	0.015	0.014	0.014	0.018
R_{sym}	0.016	0.015	0.009	0.008	0.011	0.007	0.009	0.011	0.011	0.025
Na (apfu)	0.05	0.18	0.20	0.25	0.26	0.29	0.30	0.41	0.47	0.55

imply a different origin (Caporuscio and Smyth, 1990). The inverse correlation between Na and total REE^{3+} contents also suggests the importance of electrostatic site potential constraints. This proposal is further substantiated by comparing cation electrostatic site energies of M2, because it is energetically favorable for the REE^{3+} to enter a site that has a greater electrostatic site potential. Cation electrostatic potential calculations for the M2 site in clinopyroxenes (Smyth and Bish, 1988; Caporuscio and Smyth, 1990) actually show a marked increase in going from Ca-Tschermak (−21.14 v) and diopside (−20.77 v) to jadeite (−13.57 v).

X-ray analysis and structure refinement (XRef)

Unaltered clinopyroxene single crystals were selected from crushed samples. Diffraction relations were examined by means of a Philips PW 1100 four-circle automated diffractometer with graphite monochromatized Mo*K*α radiation ($\lambda = 0.7107$ Å). All specimens examined belong to space group *C*2/*c* on the basis of the systematic absence of the $h + k =$ odd reflections. Unit-cell dimensions were calculated by means of least-squares refinement of the *d* values for 40 rows of reciprocal space by measuring the center of gravity of each reflection in the θ range 2–35° together with that measured for the same reflection at negative θ values. Unit-cell dimensions were measured for a few specimens in each rock sample, and diffraction data from at least two crystals were obtained for some rock samples to ensure major element homogeneity. The results were comparable within the estimated standard deviations; therefore the results from only one of the data sets are reported in Tables 3–6.

Technical details of data measurement and reduction have been extensively described by Ungaretti (1980) and Ungaretti et al. (1983). Two equivalent sets of reflections were measured in the θ range 2–30° by using a step scan profile technique (Lehman and Larsen, 1974); they were merged after correction for absorption (North et al., 1968) and Lp factors. The structure refinements were performed without chemical constraints. Fully ionized scattering factors were used for the non tetrahedral cations, whereas both neutral and ionized scattering factors were used for

Table 4. Bond lengths (Å) and angles (°) for cation sites

	SRV 4	SBB 7P	SBB 37	SBB 34	SBB 3H	SBB 39	SBB 25	SBB 61	XM 37	SBB 2H
T-O1	1.604	1.608	1.609	1.609	1.611	1.612	1.611	1.618	1.622	1.623
T-O2	1.588	1.592	1.589	1.588	1.590	1.589	1.589	1.590	1.592	1.594
T-O3	1.666	1.660	1.658	1.653	1.656	1.651	1.651	1.647	1.646	1.647
T-O3	1.683	1.677	1.674	1.669	1.672	1.664	1.667	1.661	1.659	1.661
⟨T-O⟩	1.635	1.634	1.633	1.630	1.632	1.629	1.629	1.629	1.630	1.631
Vol.	2.22	2.22	2.22	2.21	2.21	2.20	2.20	2.20	2.20	2.21
TAV	26.28	23.71	24.36	22.48	24.07	21.83	22.56	22.97	23.47	24.09
TQ*E*	1.006	1.005	1.006	1.005	1.006	1.005	1.005	1.005	1.005	1.006
M1-O1	2.122	2.110	2.108	2.107	2.093	2.103	2.092	2.057	2.050	2.043
M1-O1	2.057	2.042	2.031	2.028	2.025	2.023	2.017	1.990	1.985	1.982
M1-O2	2.047	2.023	2.010	2.002	1.996	1.989	1.984	1.945	1.937	1.933
⟨M1-O⟩	2.075	2.058	2.050	2.046	2.038	2.038	2.031	1.997	1.991	1.986
Vol.	11.83	11.52	11.37	11.31	11.17	11.17	11.05	10.47	10.36	10.29
OQE	1.005	1.006	1.007	1.007	1.008	1.008	1.008	1.010	1.011	1.011
OAV	17.84	20.24	21.74	22.05	24.27	23.58	24.76	32.26	34.02	34.51
M2-O1	2.360	2.367	2.360	2.341	2.365	2.332	2.348	2.365	2.369	2.376
M2-O2	2.335	2.341	2.333	2.318	2.354	2.311	2.334	2.372	2.380	2.390
M2-O3	2.562	2.538	2.528	2.533	2.514	2.522	2.508	2.461	2.457	2.450
M2-O3	2.726	2.731	2.738	2.760	2.735	2.778	2.756	2.733	2.730	2.715
⟨M2-O⟩	2.496	2.494	2.490	2.488	2.492	2.486	2.487	2.483	2.484	2.483
Vol.	25.68	25.60	25.45	25.34	25.52	25.21	25.29	25.18	25.20	25.17

Note: Tetrahedral and octahedral angular variance (TAV and OAV) and quadratic elongation (TQE and OQE) following Robinson et al. (1971); estimated standard deviations (esd) are ≤1 on the last digit.

TABLE 5. A comparison between EMP analyses, XRef results, and the calculated site populations reported in Table 6

	m.a.n. (M1 + M2)		M1 site		M2 site		⟨M1-O⟩	
	EMP	XRef	XRef	calc.	XRef	calc.	XRef	calc.
SRV-4	32.65	32.87	13.19	13.01	19.68	19.65	2.075	2.071
SBB-7P	32.00	32.15	13.96	13.85	18.19	18.06	2.058	2.057
SBB-37	30.93	30.75	13.24	13.39	17.51	17.48	2.050	2.052
SBB-34	31.83	31.84	14.16	14.04	17.68	17.61	2.046	2.048
SBB-3H	30.68	31.26	13.91	13.64	17.35	17.26	2.038	2.039
SBB-39	31.74	31.85	14.50	14.46	17.35	17.27	2.038	2.043
SBB-25	30.44	30.58	13.69	13.54	16.89	16.94	2.031	2.033
SBB-61	28.35	28.30	13.18	13.09	15.12	15.19	1.997	2.000
XM-37	29.04	28.40	13.48	13.21	14.92	14.95	1.991	1.993
SBB-2H	28.12	27.92	12.97	13.02	14.95	15.05	1.986	1.987

the tetrahedral cations and the O atoms (Ungaretti et al., 1983). The M2′ split position for Mg and Fe^{2+} has been detected for all specimens except SBB-2H and XM-37, and the occupancy and coordinates have been refined as described by Rossi et al. (1987).

Difference Fourier syntheses calculated at the end of the structure refinements always gave the highest residual peak between Si and O, and it has been ascribed to electrons concerned with covalent bonding. Final unweighted *R* indexes for the observed reflections $[I > 5\sigma(I)]$ are in the range 1.0–1.6% and are listed in Table 3, along with unit-cell dimensions and selected crystal data. Details of polyhedral geometry are reported in Table 4. Atomic coordinates and equivalent thermal factors for each specimen are reported in Appendix 2; the observed and calculated structure factors are given in Table 7.[1]

Determination of the crystal-chemical formulae

The accurate determination of the site populations for these mantle clinopyroxenes is not a simple task because of four reasons: (1) the disorder of Fe^{2+} and Mg between the M1 and M2 sites, (2) the difficulty of estimating the Fe^{2+}/Fe^{2+} ratio, (3) the presence of minor amounts of elements such as Mn, Cr, and Ti whose crystal-chemical roles are not yet clear, and (4) the presence of vacancies (□) at the M2 site.

EMP analysis provides an estimate of the amounts of cations per formula unit; however, these estimates can be biased by the presence of light elements (e.g., Li, Be) which are not detectable by EMP. Problems may also arise from the presence of microinclusions or of microstructures that are detectable only at the TEM scale.

These problems become more important when EMP analyses suggest that the M2 site is partially vacant. McCormick (1986), dealing with other clinopyroxene specimens from the Bellsbank and Robert Victor diamond mines, excluded (by means of an ion probe analysis) the presence of light elements that could have escaped detection by EMP analysis. That author also excluded (by means of TEM analysis) the presence of relevant amounts of multiple silicate chains, which would have affected the formulae (Veblen and Buseck, 1981).

XRef can provide independent evidence regarding accurate formulae. The three major controls are as follows:

1. The determination of the mean atomic numbers (m.a.n.) obtained from the structure refinement, which take into account all the chemical elements that are present in the clinopyroxene structure. This assures that light elements are not disregarded and eliminates any contribution from crystalline phases other than clinopyroxene.
2. The analysis of the diffraction profiles and the inspection of the diffraction features that are diagnostic of the presence of multiple chains in the clinopyroxene (e.g.,

TABLE 6. Site populations (apfu) for six O atoms

	M2					M1						T	
	Ca	Na	Fe^{2+}	Mg	□	Mg	Fe^{2+}	Fe^{3+}	Al	Ti	Cr	Si	Al
SRV-4	0.91	0.05	0.03	0.01	—	0.90	0.02	0.05	0.03	—	—	1.97	0.03
SBB-7P	0.78	0.18	—	0.04	—	0.79	—	0.05	0.07	—	0.09	1.97	0.03
SBB-37	0.71	0.20	—	0.09	—	0.74	0.05	0.03	0.17	0.01	—	1.98	0.02
SBB-34	0.61	0.25	0.07	0.07	—	0.65	0.10	0.03	0.22	—	—	2.00	—
SBB-3H	0.65	0.26	0.04	0.03	0.02	0.62	0.09	—	0.28	0.01	—	2.00	—
SBB-39	0.52	0.29	0.10	0.09	—	0.57	0.14	0.01*	0.27	0.01	—	2.00	—
SBB-25	0.55	0.30	0.07	0.06	0.02	0.59	0.08	—	0.32	0.01	—	2.00	—
SBB-61	0.47	0.41	0.04	0.02	0.06	0.44	0.03	—	0.52	0.01	—	2.00	—
XM-37	0.45	0.47	0.03	—	0.05	0.40	0.01	0.03	0.55	0.01	—	1.97	0.03
SBB-2H	0.45	0.55	—	—	—	0.37	—	0.03	0.60	—	—	1.92	0.08

* Mn.

---

[1] A copy of Table 7 may be ordered as Document AM-91-464 from the Business Office, Mineralogical Society of America, 1130 Seventeenth Street NW, Suite 330, Washington, DC 20036, U.S.A. Please remit $5.00 in advance for the microfiche.

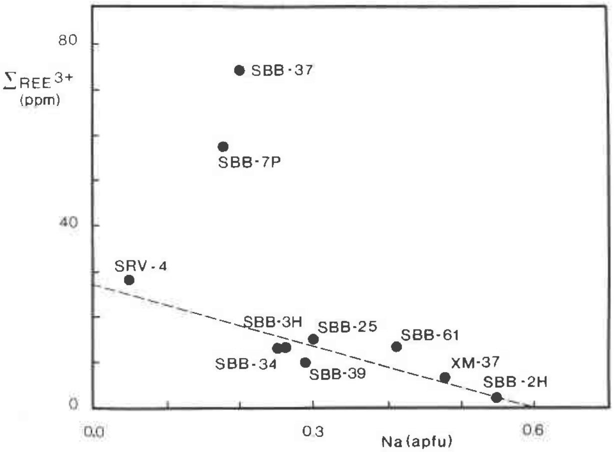

Fig. 2. A plot of total lanthanide elements whose primary oxidation state is 3+ vs. the Na content at the M2 site. The equation for the dashed line (R = 0.913) has been calculated excluding specimens SBB-7P and SBB-37.

shoulders in 00l reflections and weak and off-centered forbidden $h + k$ odd reflections that would occur in the case of amphibole lamellae). These data can be used to exclude or to estimate their presence approximately (Mellini et al., 1983).

3. The geometric description of the clinopyroxene structure (unit-cell dimensions, individual and mean cation-O bond lengths, indexes of polyhedral distortion). Those relations, combined with a definition of the crystal-chemical behavior of the cations, provide useful constraints on the determination of the site populations. In particular, sound arguments can be given for estimates of the Fe^{2+} and Fe^{3+} contents because these two cations have significantly different cation-O distances (2.130 Å in hedenbergite and 2.025 Å in acmite, Cameron et al., 1973), and the estimated error for bond distances in high-quality refinements like these is less than 0.001 Å.

The diffraction profiles of the specimens under investigation were clean and sharp (average scan widths of 2.0 to 3.0° were used), and no evidence of other diffracting phases was found. The structure refinements ended with m.a.n. for the M1 + (M2 + M2′) sites in good agreement with those calculated from the EMP analyses (Table 5). The mean value of δ = m.a.n. (XRef) − m.a.n. (EMP) is, in fact, equal to 0.007 electrons.

The site populations were, therefore, determined by taking into account both the EMP analyses and the XRef results. An iterative procedure was followed, which involves the following steps: (1) Determination of the $^{[4]}$Al content using EMP data interpreted using the observed values for ⟨T-O⟩ and ⟨M1-O⟩ mbl (see below), the construction of which involved only geometrical parameters. (2) Calculation of the site population at M2 using the values of $(Ca + Na + \square)_{EMP}$ and using the value of m.a.n.$_{XRef}$ to estimate Fe^{2+} + Mg. The value of K_{EMP} was not taken into account based on conclusions of Mellini and Cundari (1989), who demonstrated that K does not substitute in clinopyroxene; it was found to occur in amorphous microdomains that probably resulted from trapped residual liquid. (3) Verification that the remaining cation contents (Al_{tot} − $^{[4]}$Al, Fe_{tot} − Fe^{2+}_{M2}, Mg_{tot} − Mg_{M2}, Ti, Cr, Mn) fit the constraints obtained from crystal chemical relations (i.e., full occupancy of M1 and overall charge balance of the formula) and those obtained from XRef [i.e., observed m.a.n. and mean bond length (mbl)]. A satisfactory solution for x = Mg, y = Al, z = (Fe^{2+} + Mn), and w = Fe^{3+} can be obtained by solving the following system of equations:

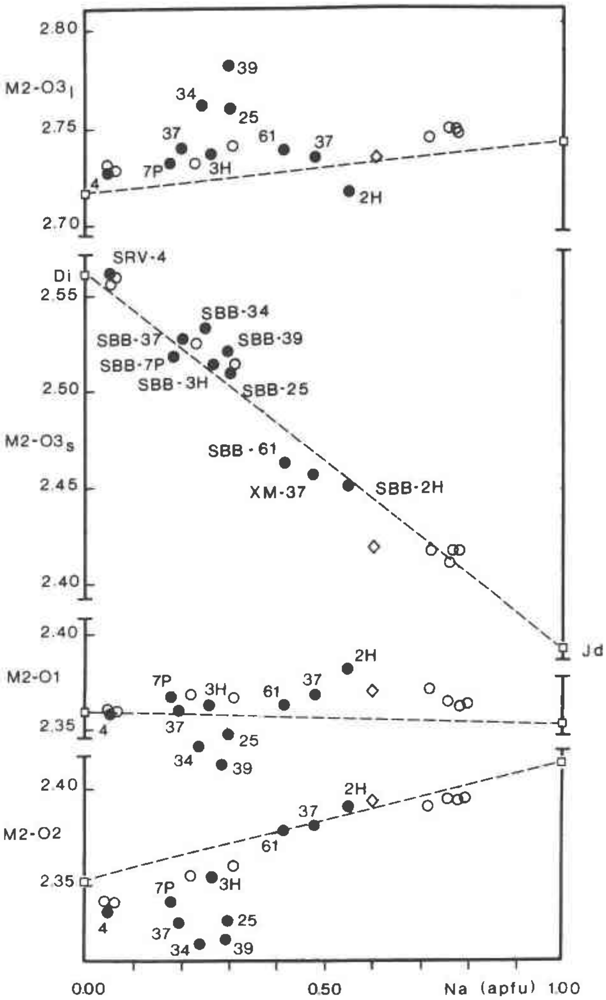

Fig. 3. The variations shown by the M2-O individual bond lengths vs. the Na content at M2. Black dots refer to the specimens in this study. Open symbols indicate data from the literature; squares = diopside (Clark et al., 1969) and jadeite (Cameron et al., 1973); circles = $C2/c$ metamorphic omphacite samples from eclogitic rocks (Rossi et al., 1983); diamonds = the M2 vacancy-bearing clinopyroxene refined by McCormick (1986). The subscripts s and l refer respectively to the shorter and the longer of the two M2-O3 distances.

$$x + y + z + w = 1 - (Ti + Cr)$$

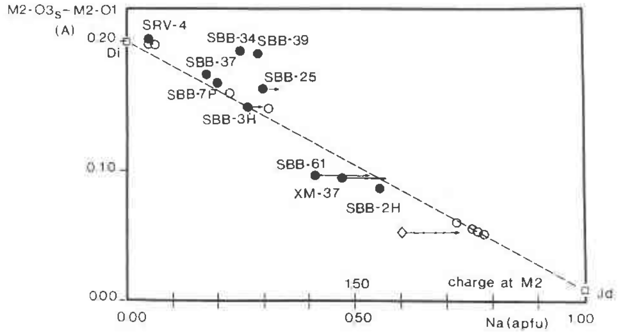

Fig. 4. The difference in bond lengths ($M2\text{-}O3_s - M2\text{-}O1$), i.e., a function of distortion in the M2 site, allows one to discriminate between the effects of the presence of $(Fe^{2+} + Mg)_{M2'}$ (cf. SBB-25, SBB-34, SBB-39) and that from the presence of vacancies (cf. XM-37, SBB-2H, SBB-61). Same symbols as in Figure 3. Arrows refer to the shifts of the vacancy-bearing specimens in shifting from the lower to the upper scale [cation charge at M2, equal to 2 × (Ca + Fe + Mg) + 1 × Na].

$$\begin{aligned}
&12x + 13y + 26z + 26w = \text{m.a.n.} - (22\ \text{Ti} + 24\ \text{Cr})\\
&2x + 3y + 2z + 3w\\
&\quad = 12 - (\text{charge at M2} + \text{charge at T} + 4\ \text{Ti} + 3\ \text{Cr})\\
&2.077x + 1.929y + 2.130z + 2.025w\\
&\quad = \text{mbl} - (1.958\ \text{Ti} + 1.998\ \text{Cr})
\end{aligned}$$

where the values in the last equation are the octahedral mbl reported, respectively, for diopside, acmite, and ureyite by Clark et al. (1969) and for jadeite and hedenbergite by Cameron et al. (1973); the value 1.958 Å was used for ⟨Ti-O⟩ by analogy with results for the sphene mineral group (Oberti et al., 1991). (4) Reiteration of the procedure from step 2 to minimize discrepancies, bearing in mind that the overall charge balance of the formula, the full occupancy of the T and M1 sites, and the observed mbl are the most important constraints. The results of this procedure for the samples under examination are reported in Table 6.

DISCUSSION OF XREF RESULTS

The crystal chemical relations for the mantle clinopyroxenes under investigation are discussed and compared with those of metamorphic specimens that are on the Di-Jd join; reference points in Figures 3–9 have been obtained for diopside (Clark et al., 1969), for jadeite (Cameron et al., 1973), and for *C2/c* omphacite samples of eclogite-facies metamorphic origin (Rossi et al., 1983). These latter reference points are useful because some crystal-chemical features exhibit nonlinear behavior in the Di-Jd system. Particular emphasis is put on the peculiarities of vacancy-bearing clinopyroxenes, with the aim of clarifying their crystal chemical relations.

The M2 site

A chemical variable was sought that could best model the effects of three different chemical substitutions [Ca → Na, Na → □, and Ca → (Fe^{2+}, Mg)] occurring at the M2 site. The use of the Na/(Ca + Na) ratio (McCormick, 1986) would neglect the role of the (Fe^{2+} + Mg) content, which will be shown to be relevant. When using the Na content in apfu, two different and concomitant phenomena can be inferred from plots of individual M2-O bond distances (Fig. 3). The more relevant of the two relations results from the presence of (Fe^{2+} + Mg), which has been shown by Rossi et al. (1987) to order in a split M2′ position (approximately 0.40 Å along **b** and toward O1 and O2, i.e., in the position and with the sixfold coordination observed in clinoenstatite and in clinoferrosilite); this position allows a more suitable coordination for the smaller ionic radii of Fe^{2+} and Mg, but results in a significant change in the charge distribution for the coordinating O atoms. This, in turn, is expected to cause changes in the polyhedron geometry. In fact, when the average site geometry obtained from XRef is taken into account, the specimens with the highest $(Fe^{2+} + Mg)_{M2'}$ contents (SBB-39, SBB-34, and SBB-25) show the highest negative deviations from the expected trend of the two shorter M2-O1 and M2-O2 bond distances. The highest positive deviations are shown for the same specimens in the two longer $M2\text{-}O3_s$ and $M2\text{-}O3_l$ bond distances. All the observed deviations are approximately proportional to the extent of the Ca → (Fe^{2+}, Mg) substitution. The effect of vacancies is different and much more subtle. For the specimen in which it prevails on that of the Ca → (Fe^{2+} + Mg) substitution (SBB-61 and XM-37), a slight increase in the M2-O2 distance with respect to the trend observed for natural samples on the Di-Jd join is observed, together with contraction in the $M2\text{-}O3_s$ distance.

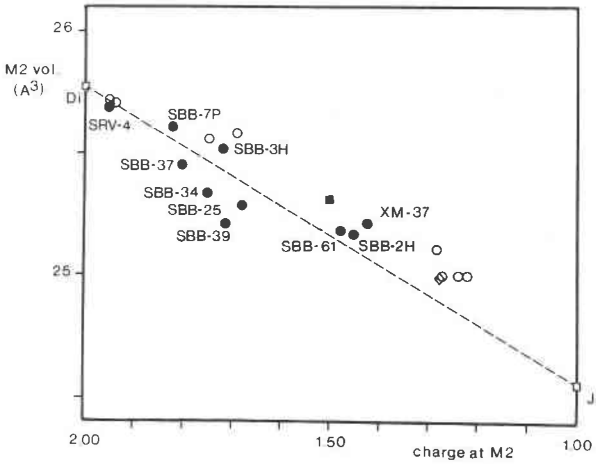

Fig. 5. The volume of the M2 polyhedron plotted against the charge of the constituent cations shows significant contraction because of $(Fe^{2+} + Mg)_{M2'}$ occupancy, as it relates to the trend observed in the Di-Jd join; no significant effect results from the presence of vacancies. Black square refers to a vacancy-bearing specimen from a grospydite in the Zagadochnaya kimberlite pipe (M.C. Domeneghetti, personal communication); the other symbols are the same as in Figure 3.

The two patterns of change in site geometry are even

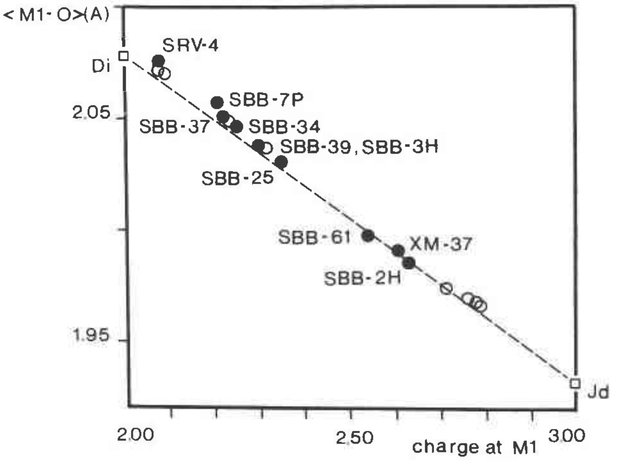

Fig. 6. The correlation between the M1-O mbl and the cation charge at the same site. Same symbols as in Figure 3.

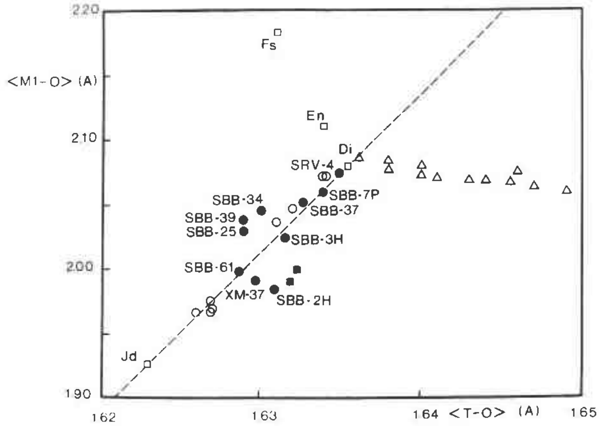

Fig. 7. Mean M1-O bond lengths vs. mean T-O bond lengths. The T-O mbl in omphacites depends on the M1-O mbl (modified from Rossi, 1988), thus making the evaluation of the [4]Al contents more complex than for calcic clinopyroxenes. Open triangles = calcic clinopyroxenes with increasing [4]Al contents (Dal Negro et al., 1982; Oberti et al., 1983). The other symbols are the same as in Figure 3.

more evident in plots of the difference between two bond lengths [$(M2\text{-}O3)_s - (M2\text{-}O1)$] against the Na content (Fig. 4, lower scale). Indeed, when the positive charge at the M2 site (calculated as 2 × (Ca + Fe + Mg) + 1 × Na) (units are atoms pfu) is used as abscissa (Fig. 4, upper scale), the plotted positions of the vacancy-bearing specimens shift to the positions marked by the points of the arrows and, therefore, fall on the trend observed for metamorphic eclogitic clinopyroxenes on the Di-Jd join. Thus, the mean cation charge shared by the coordinating O atoms seems to be the most reasonable parameter for interpretations of changes in the clinopyroxene structure; problems can, however, arise through the presence of relevant cation occupancy at the M2′ split position. Whereas the evaluation of the Na content, in the case of vacancy-bearing clinopyroxenes, is based only on EMP analyses, the cationic charge at M2 can be independently determined, both from the results of EMP analyses and from those of XRef refinement, once the cation charge at M1 is obtained from its composition (see the next paragraph). Therefore, problems deriving from uncertainties in the chemical analyses in the presence of suggested M2 vacancies should be overcome through plots against charge at M2.

The overall effect on the M2 polyhedron volume of the chemical substitutions under investigation is shown in Figure 5. The specimens with greater $(Fe^{2+} + Mg)_{M2'}$ contents (SBB-25, SBB-34, SBB-39) show larger negative deviations from the expected values, whereas no significant change in the M2 polyhedron volume is observed for the vacancy-bearing specimens (SBB-61, XM-37) and for the specimens of McCormick (1986; open diamond) and of M. C. Domeneghetti (personal communication; black square).

The octahedral M1 site

The mbl of the M1 octahedron in clinopyroxenes can be considered as a linear combination of each individual cation content multiplied by the mbl in the respective ideal end-member (Rossi et al., 1983). The M1-O mbl calculated for the specimens under investigation tend to be slightly longer than the experimental ones (Table 5). The shorter mbl calculated for specimen SRV-4 (that with the highest diopside component) and the significant deviation shown by SBB-39 (that with the highest hedenbergite component) seem to suggest that the value used for ⟨Mg-O⟩ should be slightly increased and that used for $\langle Fe^{2+}\text{-}O\rangle$ should be slightly decreased. The use of 2.078 Å and 2.120 Å, respectively, as suggested by the study of the closely related amphibole family (L. Ungaretti, personal communication) might make the agreement between observed and calculated mbl's a bit better.

In the absence of significant octahedral Mg → Fe^{2+}, [6]Al → Fe^{3+}, and [6]Al → Cr homovalent substitutions, the M1-O mbl. is linearly correlated with the cationic charge at M1 (Fig. 6), in which the small deviations from the line observed in the case of some specimens are in fact consistent with the observed amounts of the homovalent substitutions listed above (Table 6). The cation charge at M1, in those clinopyroxene compositions in which no significant [4]Al is present, is equal to 4 minus the cation charge at M2. The presence of cation vacancies at M2 is compensated by a high-charge cation content greater than that expected based on the Na content, which results in a contraction of the M1 site volume with respect to stoichiometric clinopyroxenes with the same Na content.

The tetrahedral site

An estimation of [4]Al in clinopyroxenes with appreciable Na contents cannot simply be made by means of the T-O mbl because the latter is significantly affected by the M1-O mbl (Fig. 7). Only two of the specimens used in

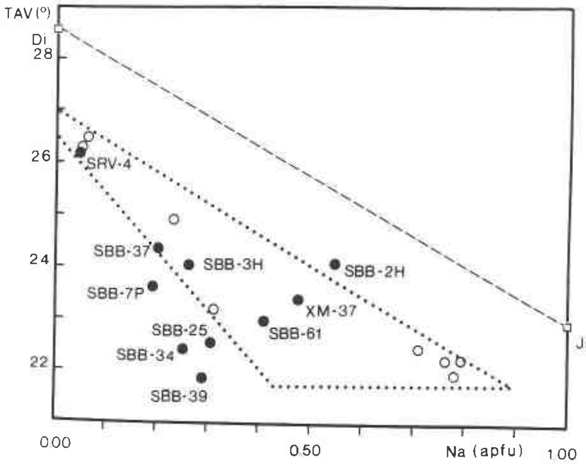

Fig. 8. Tetrahedral angular variance (TAV) vs. the Na content at M2. Dots refer to the field occupied by eclogitic *P2/n* and *C2/c* omphacites (Rossi et al., 1983).

this study (black dots) fall significantly to the right of the straight line connecting values of Jd with those of Di; therefore, they undoubtedly contain $^{[4]}$Al. The short T-O mbl's observed for specimens SBB-39, SBB-34, and SBB-25 result from their significant $(Fe^{2+} + Mg)_{M2'}$ occupancies. The presence of these substitutions increases the two M2-O3 distances; therefore, the only other bond distance involving O3 (i.e., T-O3) decreases in order to maintain the charge balance on O3. This is confirmed by the experimental points referring to orthoenstatite (En) and orthoferrosilite (Fs) (open squares), which have been calculated by averaging the (M1-O, M2-O) and (SiA-O, SiB-O) mean bond distances (Hawthorne and Ito, 1977; Sueno et al., 1976). Taking into account such relations in $(Fe^{2+} + Mg)_{M2'}$-bearing specimens, the very low amounts of $^{[4]}$Al (0.02–0.03) suggested by EMP analyses can be accepted for specimens SRV-4, SBB-7P, and SBB-37. Significant $^{[4]}$Al is present only in SBB-2H, for which the estimate of 0.08 apfu is in good agreement with the value 0.07 apfu proposed for two clinopyroxenes from the Zagadochnaya kimberlite pipe whose structures were refined using XRD data (squares in Fig. 7; M. C. Domeneghetti, personal communication).

The tetrahedral angular variances (TAV; Robinson et al., 1971) for the specimens under investigation are less than those expected for phases on the ideal Di-Jd join (Fig. 8). These specimens have space group *C2/c* and three of them fall in the range $0.3 < Na < 0.6$ that was not represented by studied specimens. They show nearly the same TAV values as those reported for the same Na contents for *P2/n* omphacites by Rossi et al. (1983). However, specimen SBB-2H has a slightly higher TAV value than expected, which is in agreement with the proposed $^{[4]}$Al content. Figure 8 also suggests that the tetrahedra of specimens with large $(Fe^{2+} + Mg)_{M2'}$ contents are more regular than those of the other specimens.

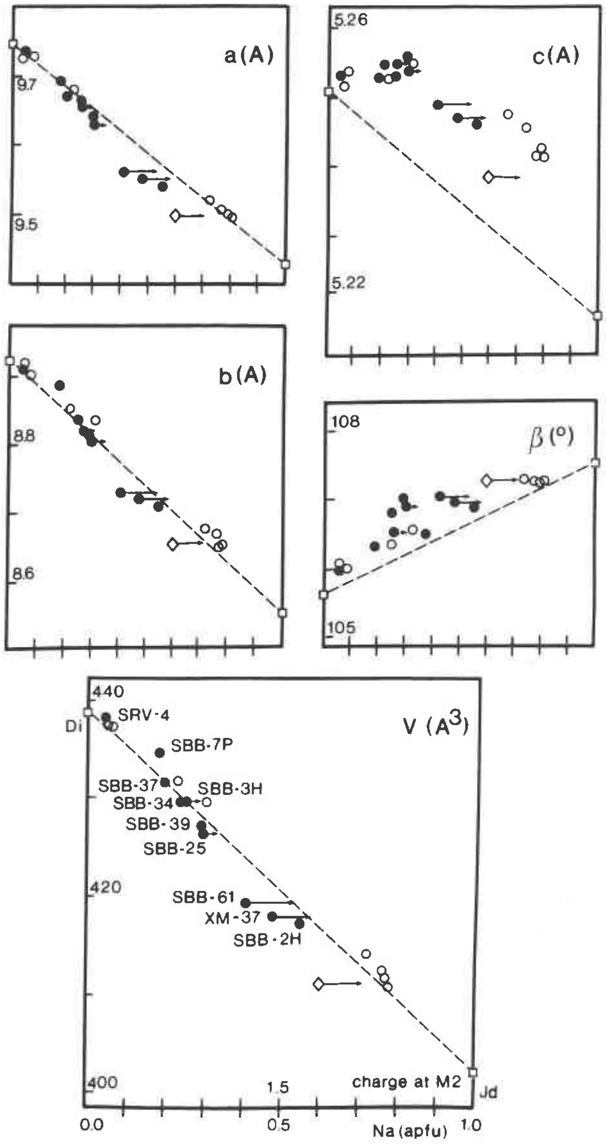

Fig. 9. Unit-cell dimensions as a function of the Na content and of the cation charge at M2. Same symbols as in Figure 3.

This study, therefore, confirms that all of the Al of clinopyroxenes of omphacitic composition tends to be in octahedral coordination. This behavior had been previously established by Rossi (1988) for *P2/n* eclogitic omphacites equilibrated at *T* up to 750 °C; it is now shown to be valid also for the *C2/c* specimens which equilibrated at *T* between 950 and 1200 °C and which were investigated in this study. The presence of Al with the highest coordination number possible for the clinopyroxene structure is in agreement with the high *P* of reequilibration. The highest amounts of $^{[4]}$Al (never exceeding 0.10 apfu) are found in specimens from grospydites, consistent with their bulk compositions, high *T* of crystallization, and quenching during uplift.

Unit-cell dimensions and space group

All the omphacitic specimens of this study have space group *C*2/*c*; no traces of incipient ordering as occurs with space group *P*2/*n* have been found during X-ray analysis. This is in agreement with the estimated temperatures of recrystallization (950–1200 °C), which are well above the temperature of 850 °C inferred by Carpenter (1981) for complete transition from a structure with space group *C*2/*c* to one with space group *P*2/*n*.

Unit-cell dimensions have been plotted against the composition of the M2 site in order to determine if the dimensions are affected by the presence of vacancies. If the positive charge at M2 is used as abscissa (Fig. 9, upper scale; cf. the points of the arrows), it is evident that the dependence of *a, b,* and *V* with the Na content is reasonably linear for samples on the Di-Jd join, whereas variations in *c* and β deviate significantly from linearity. The *c* unit-cell dimension strongly depends on the geometry of the tetrahedron, which has already been shown to vary in a nonlinear way along the Di-Jd join. It is worth noting that the β angle is significantly affected by the $(Fe^{2+} + Mg)_{M2'}$ content.

It is useful to analyze the changes in the unit-cell volume for these high-*P* mantle clinopyroxenes in more detail. All the reference points for eclogitic clinopyroxenes and the two compositions that are more diopsidic fall on the right of the Di-Jd line; this is because the significant Mg → Fe^{2+}, Al → Fe^{3+}, and Al → Cr homovalent substitutions at the M1 site all actually cause an increase in the unit-cell volume. On the other hand, the specimens with significant $(Fe^{2+} + Mg)_{M2'}$ contents have unit-cell volumes less than those predicted from their Na contents; this result is in agreement with the contraction in the M2 and T sites discussed above.

Even if vacancy-bearing pyroxenes show the unit-cell volumes predicted by the positive charge at M2 (Fig. 9, upper scale; points of the arrows), they show relevant deviations from the Di-Jd line when using the Na content (apfu) as abscissa (Fig. 9, lower scale; black dots). When EMP analyses suggest the presence of M2 vacancies in clinopyroxenes, a determination of the unit-cell dimensions can, therefore, provide a reliable check for their presence and extent. This is a straightforward method to exclude the analytical problems that have been discussed in the experimental section.

REE affinity

The slight decrease in the M2 site volume with increase in Na content shown by the studied samples is in agreement with the LREE depletion shown in Figure 1. However, as discussed in the introduction, on the basis of the ionic radii, the decrease is too small to induce LREE depletion. On the other hand, the presence of significant $(Fe^{2+} + Mg)_{M2'}$ substitutions has been shown to affect more significantly the volume and distortion of the M2 polyhedron than the Na content does. Specimens with high $(Fe^{2+} + Mg)_{M2'}$ contents actually have smaller LREE values in Figure 1. However, it must be remembered that the description of the polyhedron geometry determined by XRef is an average over the full volume of the crystal examined. This masks atomistic effects at the unit-cell level; it is not possible, therefore, to discard the hypothesis that the LREE (concentrations on the order of ppm) substitute into a region of the crystal, if any, that is particularly Ca rich.

The role of the M2 site population in very high pressure clinopyroxenes

The main crystal-chemical peculiarities of the clinopyroxenes under investigation involve the M2 site compositions. Chemical substitutions for both Ca and Na are observed: Ca → (Fe^{2+}, Mg) and Na → □. The former substitution induces a change in the coordination number (from eight to six) of M2, which occupies the M2′ position. This shift causes a drastic change in the charge distribution on the coordinated O atoms, which in turn affects the geometry of the other polyhedra. In particular, O3 changes from being oversaturated to being undersaturated; this induces regularization of the tetrahedral geometry, in terms of both TAV and individual T-O distances (Table 4). The final result is a decrease in the unit-cell volume.

On the other hand, the presence of vacancies at M2 does not seem to induce structure modifications different from those due to the Ca → Na substitution. (The clinopyroxenes structure in this case is affected only by the decrease in the M2 positive charge.) In detail, the crystal-chemical behavior of the vacancy-bearing specimens can be explained by the following model: The lack of a cation in the center of the M2 cavity induces a significant underbonding of the coordinated O atoms that is most critical for the nearest O atoms. This underbonding is compensated, in the case of the O1 and O2, by trivalent cations substituting for Mg and Fe^{2+} at the M1 site. The result is a strong contraction in the M1 polyhedron volume, with no relevant effects on the M2 polyhedron volume. The lack of significant volume contraction around the M2 site may be explained by the presence of Coulombic anion-anion repulsive forces which prevent the empty cavity from collapsing when no cation is present. The O3 atoms, which are shared only between the M2 and the T sites, are then undersaturated. This induces a significant lengthening of the T-O1 bond distance and a concomitant shortening of the T-O3 bond distances. Based on these considerations, $^{[4]}Al$ substitution for Si (which would further enhance the O underbonding and would require longer T-O3 distances) should be inhibited when vacancies are present at M2. The presence of very small amounts of $^{[4]}Al$ and associated vacancies (both with concentrations less than 0.10 apfu) in some mantle clinopyroxenes (see also Sobolev, 1977; Smith et al., 1982; Smyth, 1980; McCormick, 1986) can be explained by (1) the extremely high *T* of crystallization (which also allows the presence of $^{[4]}Al$ at high *P*) and (2) the fact that these two substitutions are not simultaneously present in neighboring M2 and T sites. Vacancies are most likely to substitute following the reaction $\mathrm{Na}_{\mathrm{M2}} + \mathrm{R}^{2+}_{\mathrm{M1}} \rightarrow \square_{\mathrm{M2}} + \mathrm{R}^{3+}_{\mathrm{M1}}$, which results in the formation of a stable and very compact clinopyroxene and makes some Na available for the subsequent crystallization of very compact clinopyroxenes.

The observed substitutions for Na and Ca at the M2 site both result in decreased unit-cell volumes and can thus be related to the extremely high *P* conditions of crystallization of the specimens in this study.

ACKNOWLEDGMENTS

This article has greatly benefited from early review by L. Ungaretti; we thank him very much. We also acknowledge the careful and skillful review of the paper by T.C. McCormick. Thanks are also due to M.C. Domeneghetti, who made her unpublished data on vacancy-bearing clinopyroxenes available for comparison. Analyses by INAA of REE were completed with the help of W. Boynton and D. Hill (University of Arizona). Supplemental REE determinations for sample SBB-2H were obtained with the help of R. Vannucci and P. Bottazzi (C.S. Cristallografia Strutturale, Pavia). Major element analyses were performed at Los Alamos National Laboratory with the help of R. Hagen. Partial funding of REE INAA was supplied by NSF grant EAR-8709224 to J.R. Smyth. One of the authors (F.A.C.) is grateful to the Consiglio Nazionale delle Ricerche, Italy, for funding his travel and research time in Pavia (grant C/106018/058803664).

REFERENCES CITED

Boynton, W.V. (1979) Neutron activation analysis. In D.A. Gscheidner and L. Eyring, Eds., Handbook on the physics of rare earths, vol. 4: Non-metallic compounds II, p. 457–470. North-Holland, Amsterdam.

Cameron, M., Sueno, S., Prewitt, C.T., and Papike, J.J. (1973) High temperature crystal chemistry of acmite, diopside, hedenbergite, jadeite, spodumene, and ureyite. American Mineralogist, 58, 594–618.

Caporuscio, F.A. (1988) Petrogenesis of mantle eclogites from South Africa, 148 p. Ph.D. dissertation, University of Colorado, Boulder, Colorado.

Caporuscio, F.A., and Smyth, J.R. (1986) Rare earth signature of garnet and clinopyroxene from mantle eclogites. Eos, 67, 1395.

——— (1990) Trace element crystal-chemistry of mantle eclogites. Contributions to Mineralogy and Petrology, 105, 550–561.

Carpenter, M.A. (1981) Time-temperature-transformation (TTT) analysis of cation disordering in omphacites. Contributions to Mineralogy and Petrology, 78, 433–440.

Clark, J.R., Appleman, D.E., and Papike, J.J. (1969) Crystal-chemical characterization of clinopyroxenes based on eight new structure refinements. Mineralogical Society of America, Special Paper 2, 31–50.

Dal Negro, A., Carbonin, S., Molin, G.M., Cundari, A., and Piccirillo, E.M. (1982) Intracrystalline cation distribution in natural clinopyroxenes of tholeitic, transitional and alkaline basalts. In S.K. Saxena, Ed., Advances in physical geochemistry, vol. 2, p. 117–150. Springer, New York.

Dal Negro, A., Carbonin, S., Domeneghetti, C., Molin, G.M., Cundari, A., and Piccirillo, E.M. (1984) Crystal-chemistry and evolution of the clinopyroxenes in a suite of high pressure ultramafic nodules from the newer volcanics of Victoria, Australia. Contributions to Mineralogy and Petrology, 86, 221–229.

Dawson, J.B. (1980) Kimberlites and their xenoliths, 252 p. Springer-Verlag, New York.

Dawson, J.B., and Gurney, J.J. (1987) Roberts Victor eclogites and their relations to the mantle. In P.H. Nixon, Ed., Mantle xenoliths, p. 453–463. Wiley, New York.

Early, T.O. (1971) Rare earths in eclogites from the Roberts Victor kimberlite, South Africa. Contribution 2144, Publication Division of Geologic and Planetary Sciences, California Institute of Technology, Pasadena, California.

Hanson, G.N. (1980) Rare earth elements in petrogenetic studies of igneous systems. Annual Review of Earth and Planetary Sciences, 8, 371–406.

Hawthorne, F.C., and Ito, J. (1977) Synthesis and crystal-structure refinement of transition metal orthopyroxenes. I. Orthoenstatite and (Mg, Mn, Co) orthopyroxene. Canadian Mineralogist, 15, 321–338.

Irving, A.J. (1978) A review of experimental studies of crystal/liquid trace element partitioning. Geochimica et Cosmochimica Acta, 42, 743–770.

Lehman, M.S., and Larsen, F.K. (1974) A method for location of the peaks in step-scan measured Bragg reflections. Acta Crystallographica, A24, 351–359.

McCormick, T.C. (1986) Crystal-chemical aspects of nonstoichiometric pyroxenes. American Mineralogist, 71, 1434–1440.

McCormick, T.C., and Smyth, J.R. (1986) Geothermometry and geobarometry for kyanite eclogites from Bellsbank and Roberts Victor mine kimberlites. Fourteenth General Meeting of the International Mineralogical Association, Abstracts, 169. Stanford, California.

Mellini, M., and Cundari, A. (1989) On the reported presence of potassium in clinopyroxene from potassium-rich lavas: A transmission electron microscope study. Mineralogical Magazine, 53, 311–314.

Mellini, M., Oberti, R., and Rossi, G. (1983) Crystal-chemistry and microstructures of pyroxenes and amphiboles in the corona of the Bergen Arcs and of the Sognefjord region, Western Norway. Periodico di Mineralogia, 52, 583–615.

North, A.C.T., Philips, D.C., and Mathews, F.S. (1968) A semi-empirical method of absorption correction. Acta Crystallographica, A24, 351–359.

Oberti, R., Munno, R., Foresti, E., Krajewsky, A. (1983) A crystal-chemical study on six fassaites from the Predazzo Monzoni area. Rendiconti della Società Italiana di Mineralogia e Petrologia, 38, 649–655.

Oberti, R., Smith, D.C., Rossi, G., Caucia, F. (1991) The crystal-chemistry of high-aluminium titanites. European Journal of Mineralogy (in press).

Prewitt, C.T. (1980) Pyroxenes. In Mineralogical Society of America Reviews in Mineralogy, 7, 525 p.

Robinson, K., Gibbs, G.V., and Ribbe, P.H. (1971) Quadratic elongation, a quantitative measure of distortion in coordination polyhedra. Science, 172, 567–570.

Rossi, G. (1988) A review of the crystal chemistry of clinopyroxenes in eclogites and eclogite-facies rocks. In D.C. Smith, Ed., Eclogites and eclogite-facies rocks, p. 237–270. Elsevier, Amsterdam.

Rossi, G., Smith, D.C., Ungaretti, L., and Domeneghetti, M.C. (1983) Crystal-chemistry and cation ordering in the system diopside-jadeite: A detailed study by crystal structure refinement. Contributions to Mineralogy and Petrology, 83, 247–258.

Rossi, G., Oberti, R., Dal Negro, A., Molin, G.M., Mellini, M. (1987) Residual electron density at the M2 site in *C*2/*c* clinopyroxenes: Relationships with bulk chemistry and sub-solidus evolution. Physics and Chemistry of Minerals, 14, 514–520.

Shannon, R.D. (1976) Revised effective ionic radii and systematic studies of interatomic distances in halides and chalcogenides. Acta Crystallographica, A32, 751–767.

Shervais, J.W., Taylor, L.A., Lugmair, G.W., Clayton, R.N., Mayeda, T.K., Korotev, R.L. (1988) Early Proterozoic oceanic crust and the evolution of subcontinental crust: Eclogites and related rocks from southern Africa. Geologic Society of America Bulletin, 100, 411–423.

Shimizu, H. (1980) Experimental study on REE partitioning in minerals formed at 20 and 30 Kb for basaltic systems. Geochemical Journal, 14, 185–202.

Smith, D.C., Domeneghetti, M.C., Rossi, G., and Ungaretti, L. (1982) Single-crystal structure refinements of super-silicic clinopyroxenes from the Zagadochnaya kimberlite pipe, Yakutia, U.S.S.R. (abs.). Terra Cognita, 2, 223.

Smyth, J.R., (1980) Cation vacancies and the crystal chemistry of breakdown reactions in kimberlitic omphacites. American Mineralogist, 65, 1257–1264.

Smyth, J.R., and Bish, D.L. (1988) Crystal structures and cation sites of the rock-forming minerals, 332 p. Allen and Unwin, Boston.

Smyth, J.R., and Caporuscio, F.A. (1984) Petrology of a suite of eclogite inclusions from the Bobbejaan kimberlite: II. Primary phase compositions and origin. In J. Kornprobst, Ed., Kimberlites II: The mantle and crust-mantle relationships, p. 121–132. Elsevier, Amsterdam.

Smyth, J.R., Caporuscio, F.A., and McCormick, T.C. (1989) Mantle eclogites: Evidence of igneous fractionation in the mantle. Earth and Planetary Science Letters, 93, 133–141.

Sobolev, N.V. (1977) Deep-seated inclusions in kimberlites and the problem of the composition of the upper mantle, p. 280. American Geophysical Union, Washington, DC.

Sueno, S., Cameron, M., and Prewitt, C.T. (1976) Orthoferrosilite: High-temperature crystal-chemistry. American Mineralogist, 61, 38–53.

Ungaretti, L. (1980) Recent developments in X-ray single crystal diffractometry applied to the crystal-chemical study of amphiboles. Godisniak Jugoslavenskog Centra za Kristalografiju, 15, 29–65.

Ungaretti, L., Lombardo, B., Domeneghetti, C., and Rossi, G. (1983) Crystal-chemical evolution of amphiboles from eclogitised rocks of the Sesia-Lanzo Zone, Italian Western Alps. Bulletin de Minéralogie, 106, 645–672.

Veblen, D.R., and Buseck, P.R. (1981) Hydrous pyriboles and sheet silicates in pyroxenes and uralites: Intergrowth microstructures and reaction mechanisms. American Mineralogist, 66, 1107–1134.

MANUSCRIPT RECEIVED AUGUST 1, 1990
MANUSCRIPT ACCEPTED APRIL 5, 1991

APPENDIX 1. SAMPLE PETROGRAPHY

SRV-4 bimineralic eclogite. Orange-red, ovoid, garnets 5 mm in diameter displaying marked segregation and lineation are set in a matrix of light green anhedral clinopyroxene, 4–9 mm. The pyroxene has distinct sets of lamellae (possible orthopyroxene exsolution?) that have altered to unknown phases.

SBB-7P bimineralic eclogite. Emerald green, 2.5-mm anhedral clinopyroxene is intergrown with subhedral, purple garnet (6 mm).

SBB-37 bimineralic, rutile-bearing eclogite. Subhedral, light to moderate orange-red, 10-mm garnet grains form an interlocking texture with gray-green, 5-mm clinopyroxene grains. Orange to straw brown rutile is present in trace amounts.

SBB-34 bimineralic eclogite. Anhedral, moderate orange-red, garnets, 6–8 mm, are set in an interlocking pattern with subhedral, medium green clinopyroxene, 2–4 mm. There is a small amount of garnet exsolution (Smyth et al., 1989), occurring as blebs precipitated within the pyroxene.

SBB-3H bimineralic eclogite. Pink 10-mm garnets are set in an interlocking matrix with medium dark green, 12-mm clinopyroxene. Oriented precipitation (exsolution lamellae?) of garnet, 0.6 × 0.1 mm, and phlogopite, 2.0 × 0.1 mm, are rarely observed in larger clinopyroxene grains.

SBB-39 bimineralic eclogite. Rounded, 3-mm orange-red garnets are oriented in layers in a light green interlocking matrix of 7-mm clinopyroxenes. Rarely, phlogopite blebs occur within pyroxene grains. The mica is not in optical continuity or aligned within the pyroxene. The blebs appear to be secondary replacement features.

SBB-25 bimineralic eclogite. Rounded, moderate red, 4-mm garnets in defined layers are set in a gray-green, granular clinopyroxene matrix, 1–3 mm. The pyroxene commonly exhibits preferential alteration along defined planes to an unidentified assemblage of secondary phases.

SBB-61 bimineralic eclogite. Sub- to euhedral, medium red, 4-mm garnets meshed in an interlocking fabric with dark gray-green, subhedral, 3-mm clinopyroxene. Rare garnet blebs occur in pyroxene. Their orientation is unknown, but they seem to have a preferred alignment.

XM-37 bimineralic, rutile-bearing eclogite. Subhedral medium orange-red garnet, 2.5–5.0 mm, and rare, anhedral, yellow-brown, 0.5-mm rutile, both showing moderate lineation, are set in an interlocking matrix of dark green clinopyroxene, 1.5–3.0 mm.

SBB-2H corundum-bearing grospydite. Pink-orange anhedral garnet, 3–4 mm, and blue, euhedral, twinned kyanite, 0.6–1.5 mm, are set in a matrix of very light green, turbid, clinopyroxene, 3–4 mm. Pink corundum occurs as both 0.5-mm primary blebs (in all three phases) and secondary needles separating kyanite and clinopyroxene. Both garnet and kyanite are also seen as exsolution lamellae in some clinopyroxene grains.

APPENDIX 2. Atomic fractional coordinates (×10^4) and equivalent thermal factors (Å^2) for the specimens of this study (esd $\leq$ 1 on the last digit)

		SRV 4	SBB 7P	SBB 37	SBB 34	SBB 3H	SBB 39	SBB 25	SBB 61	XM 37	SBB 2H
O1	*x*	1156	1150	1146	1148	1139	1146	1141	1120	1115	1112
	y	870	853	848	844	835	837	832	805	797	797
	z	1421	1405	1388	1395	1381	1393	1379	1339	1331	1324
	B	0.51	0.61	0.80	0.86	0.85	0.93	0.84	0.83	0.85	0.73
O2	*x*	3616	3614	3616	3621	3608	3626	3617	3606	3605	3604
	y	2501	2519	2523	2524	2535	2532	2539	2569	2574	2580
	z	3195	3170	3175	3179	3134	3178	3147	3067	3051	3039
	B	0.71	0.78	0.98	1.07	0.92	1.17	0.99	0.89	0.89	0.73
O3	*x*	3509	3513	3515	3517	3515	3522	3520	3523	3523	3524
	y	178	168	163	160	154	151	149	130	126	127
	z	−39	−19	−7	17	−9	44	23	12	7	−6
	B	0.56	0.59	0.74	0.79	0.70	0.87	0.73	0.69	0.69	0.58
T	*x*	2869	2877	2879	2886	2876	2892	2886	2886	2886	2884
	y	930	927	927	924	928	922	925	928	928	931
	z	2304	2309	2312	2331	2298	2347	2322	2290	2282	2269
	B	0.33	0.35	0.50	0.49	0.47	0.55	0.46	0.43	0.44	0.34
M1	*x*	0	0	0	0	0	0	0	0	0	0
	y	9075	9068	9060	9056	9059	9051	9055	9056	9055	9061
	z	2500	2500	2500	2500	2500	2500	2500	2500	2500	2500
	B	0.42	0.46	0.58	0.63	0.59	0.63	0.53	0.42	0.52	0.39
M2	*x*	0	0	0	0	0	0	0	0	0	0
	y	3007	3008	3003	2973	3005	2958	2982	3006	3008	3021
	z	2500	2500	2500	2500	2500	2500	2500	2500	2500	2500
	B	0.67	0.76	0.85	0.96	0.89	1.07	0.91	0.85	0.87	0.77
M2′	*x*	0	0	0	0	0	0	0	0		
	y	2419	2498	2454	2411	2387	2452	2448	2386		
	z	2500	2500	2500	2500	2500	2500	2500	2500		
	B	0.49	0.64	0.58	0.30	0.75	0.42	0.15	1.06		